OPEN ACCESS
IOP Publishing
Semiconductor Science and Technology
Semicond. Sci. Technol. **29** (2014) 064003 (7pp)
doi:10.1088/0268-1242/29/6/064003

Thermopower engineering of Bi_2Te_3 without alloying: the interplay between nanostructuring and defect activation

Changdeuck Bae[1,2], Tim Böhnert[1], Johannes Gooth[1], Seulky Lim[2], Seonhee Lee[2], Hyunchul Kim[2], Stefan Heimann[3], Stephan Schulz[3], Hyunjung Shin[2] and Kornelius Nielsch[1]

[1] Institute of Applied Physics, University of Hamburg, Jungiusstrasse 11, D-20355 Hamburg, Germany
[2] Department of Energy Science, Sungkyunkwan University, Suwon 440-746, South Korea, and Integrated Energy Center for Fostering Global Creative Researcher (BK 21 plus), Sungkyunkwan University, Suwon 440-746, South Korea
[3] University of Duisburg-Essen, Institute of Inorganic Chemistry and Center for Nanointegration Duisburg-Essen (CENIDE), Universitätsstr. 5-7, D-45117 Essen, Germany

E-mail: cdbae@physnet.uni-hamburg.de and changdeuck@skku.edu

Received 26 November 2013, revised 29 January 2014
Accepted for publication 11 February 2014
Published 6 May 2014

Abstract

We report on the interplay between nanostructuring and defect activation in dense polycrystalline Bi_2Te_3 thin films in terms of the thermopower engineering. The Bi_2Te_3 thin films were prepared at relatively low temperatures (100–160 °C) by atomic layer deposition and their grains showed different sizes in the range of 50–200 nm according to the deposition temperatures. We monitored the conductivity, Seebeck coefficient, and power factor of all samples from the temperature of 50–400 K. By increasing the growth temperature, remarkably, we observed the gradual defect activation from the nominal *p*-type to *n*-type in our binary end compound, Bi_2Te_3 without any alloying. The present results give us an insight on the optimization of thermoelectric materials not only by nanostructuring (i.e., phonon engineering) but also by controlled defect activation (i.e., electron engineering).

Keywords: thermopower, atomic layer deposition, topological insulators

(Some figures may appear in colour only in the online journal)

1. Introduction

Optimizing thermoelectric performance is now being faced with a new era mainly due to the sustainability issue for efficient energy consumption and waste heat scavenging world-wide and to the recent developments tackling the long-standing low-efficiency ($ZT \sim 1$) by nanostructuring thermoelectric materials [1]. It is associated with the materials' dimensionless figure of merit, $ZT = S^2\sigma T/\kappa$, where S is the Seebeck coefficient, σ the electrical conductivity, T the average temperature, and κ the thermal conductivity. In order to maximize ZT, controlling the properties of thermoelectric materials is the key, however it is complex since the desired parameters are found to be interdependent, known as the Wiedemann–Franz law for metals or degenerated semiconductors [2]. For this purpose, the nanostructuring strategy has been successfully employed since the introduction by Hicks and Dresselhaus in 1993 [3]. Indeed, a certain range of the phonon spectrum could effectively be engineered by nanoscaling granular materials to a size comparable with the phonon mean free path [4, 5, 6]. Successful examples of nanograined PbTe [7], Bi_2Te_3 [8], and SiGe [9], as well as hierarchically structured PbTe [10] highlight the significance of phonon engineering. Meanwhile, systematic understanding

with controlled grain sizes has been reported rarely because the grain growth during high-temperature bulk processes makes the fine tuning difficult. To this end, oxide systems have been studied over a wide variety of grain sizes [11]. Very recently, the drop-casted films of CdSe nanoparticles without organic surfactants and their thermal conductivity were reported by varying the grain size to fall beneath the amorphous limit [12]. Nevertheless, whether or not the porosity operates in such air-particles composite system is ambiguous. Furthermore, the contribution of electronic transport on the thermal conductivity is essential and its understanding pertains to the type of defects and activation within the material.

Bi_2Te_3 is a representative, efficient thermoelectric material for near room temperature applications [13, 14]. Although there are over 60-years history about this line of research, the robust surface transport states have been found very recently in terms of the topologically protected order parameters [15, 16]. Bi_2Te_3 has a rhombohedral structure, belonging to the space group $D_{3d}^5 - R\bar{3}m$ and equivalent to a hexagonal unit cell in a more intuitive description. The ordered Te^1–Bi–Te^2–Bi–Te^1 quintuple layers constitute a unique layered structure, where the Te^1–Te^1 bond is of van der Waals' type with a gap responsible for the easy mechanical cleavage as well as the anisotropic transport properties. The band gap is narrow, ~150 meV at room temperature [17], easily making the system be degenerately doped and highly conductive. In consequence, the synergetic combination between the phonon tunneling gap and the anisotropic electron transport (probably, including topologically protected surface electronic bands) plausibly results in the desired thermoelectric performance, making Bi_2Te_3 ideal. In fact, however, the perfect stoichiometric Bi_2Te_3 as binary end compound should be a nominal *p*-type semiconductor [18] because of the low formation energy (E_a = ~0.4 eV) of anti-site defects (i.e., Bi on the Te sites, denoted by Bi'_{Te}) in accordance with the reaction, $Bi_2Te_3 \Leftrightarrow 2Bi'_{Te} + 2h^{\bullet} + Te_2(g) + Te_{Te}$ [19]. Moreover, the migration energy for the Te vacancy is also quite low (E_{Te} = ~1 eV), indicative of a high vapor pressure [20]. Therefore, the high temperature processing often results in undesired doping/inhomogeneity even though Bi_2Te_3 is an unambiguous line compound according to its phase diagram, leading to slight bismuth overstoichiometry at the gas–solid interfaces even within the same phase.

Alloying with other elements gives further opportunities in engineering thermoelectric properties. For example, alloying with Se allows for band gap tuning of well over ~300 meV [17] by subsequently substituting the -Te^2- site and by adding more ionicity in the solid solution [21]. In addition to doping with an opposite dopant, consequently, such an alloying adjusts the impurity levels in the bulk gap so that the carrier concentration is optimized. The above scenario assumes a situation where all the possible defects are activated after thermal equilibria as a result of the high temperature processing (e.g., well over 800 °C for the Bridgman techniques). The strategy to reduce the carrier concentration by alloying has been adopted in the investigation of topological insulators as well [22]. More critical are, however, the difficulties to control the doping level even within a bulk ingot from the same batch [20]. Considering the near room temperature applications, it is interesting to distinguish whether high temperature processing is really necessary or not so that uniform and controlled defect activations are possible.

Atomic layer deposition (ALD) utilizes gas-phase surface reaction carried out in a so-called self-limiting manner [23]. There are two major reasons why we employ ALD techniques for this study. One is to obtain the stoichiometric compounds as a result of the chemical reactions, and the other is to achieve lower temperatures in the materials preparation. To avoid or minimize thermal decompositions of precursor molecules, indeed, it usually employs moderate/low deposition temperatures (if not, resulting in non-stoichiometric material films). In this context, the thermal control over the defect activations is expected if the defects are likely activated within the growing temperatures. More remarkably, the resulting ALD layers might have nearly perfect stoichiometry in accordance with the designated chemistry rather than by the amount of input materials. Additionally, the slow processes of ALD could result in the materials quality prepared at the thermal equilibrium, as will be discussed later.

Beginning with Bi_2Te_3 as an example of binary end compounds, here, we report on the interplay between nanostructuring and defect activation for thermopower engineering in polycrystalline and dense Bi_2Te_3 thin films. The grain size and the amount/type of defects were systematically varied by low-temperature ALD. By increasing the growth temperature (100–160 °C), the grain sizes were tunable in the range of 50–200 nm. More remarkably, we observed the gradual activation of defects from the nominal *p*-type to *n*-type behaviors. Both effects on the thermopower were analyzed by monitoring the conductivity, the Seebeck coefficient and the power factor (PF) from 50–400 K. It is noteworthy that the present study does not aim at attaining high performance thermoelectric materials. Our results rather provide an insight on the understanding of thermoelectric properties by both nanostructuring (i.e., phonon engineering) and control of defect activation (i.e., electron engineering) without any alloying and post-annealing. This understanding is crucial for the further optimization of ZT factor, rendering high-efficiency thermoelectric materials.

2. Experimental

The substrate was cleaned with ozone in the ALD chamber prior to coating the thermoelectic layer. The Bi_2Te_3 layers were grown onto the 300 nm-thick SiO_2/Si substrate at given temperatures. The resulting films were taken out of the ALD reactor upon cooling it down to room temperature in order to minimize possible surface oxidation. The Hall bar structures (typically 200 × 2000 μm) were defined on the thermoelectic layer by photolithography and subsequent wet-chemical etching. The etchant was a diluted aqua regia (mixed with concentrated nitric acid and hydrochloric acid) solution in deionized water with a ratio of 1 : 20 v v^{-1}. Then, the electrodes for the Hall bar and the heater lines were platinized by sputtering and subsequent lift-off using pre-patterned photoresist (PR) structures. Note that the entire

processing temperatures during device fabrication such as PR baking were carefully controlled below 100 °C to avoid any unwanted defect activations and oxidation.

ALD reactions were carried out in a commercial flow-through-type reactor (TFS 200, Beneq, Finland). Bis(trimethylsilyl)telluride [24]and bismuth(III) chloride [Strem Chemicals, Inc.] were used as reactants, and were respectively kept at 50 °C and 140 °C. Ar (4N) was used as carrier as well as purging gas. Exposure times for reactants and purge times were optimized for our system. A full ALD cycle consisted of 0.3/3 s injection of $BiCl_3$/$Te(SiMe_3)_2$, respectively, and Ar purging for 30 s. Although the exposure dose for Bi would be under saturation at lower T_{sub}, optimizing T_{sub}-independent growth rates is out of the scope in this study, as will be addressed later. We rather achieved the reproducible ALD reactions by increasing the flow rate for Bi. The total flow and working pressure during ALD were ∼300–500 standard cubic centimeters per minute (sccm) and 3–6 mbar, respectively.

The resulting morphologies of Bi_2Te_3 films were investigated without coating a conductive layer by scanning electron microscopy (SIGMA, Carl Zeiss AG, Germany). The overall statistics on the grain size and thickness were calculated on the basis of more than 50 measurements. To analyze the surface morphology in detail, an ambient atomic force microscopy (AFM) was employed (SPA-400, Seiko Instrument, Japan). The AFM height images were obtained under a non-contact mode using silicon cantilevers with a spring constant of ∼42 $N \cdot m^{-1}$ at a scan rate of 0.5 Hz. The structures were characterized by x-ray diffraction (XRD, SmartLab, Rigaku, Japan) and high-resolution transmission electron microscopy (HR-TEM, JEM 2100F, JEOL, Japan).

The conductivity and Seebeck coefficient were measured in a commercial cryostat at the temperature range of 50–400 K (VersaLab, Quantum Design, Inc. CA, USA) with an external power source (E3644A, Agilent) and nanovoltmeter (2182A, Keithley). Ohmic contact between the Pt electrodes and Bi_2Te_3 layers was found as-fabricated. The film thicknesses were in the range of 50–200 nm by ALD of 1000 cycles at different growth temperatures. All the thermoelectric measurements were carried out in the dark. More detailed methods can be found in previous publications [25, 26].

3. Results and discussion

ALD of Bi_2Te_3 has been recently reported by Pore *et al* although the exact details such as the resultant structures were unfortunately not given in the publication [27]. In fact, it was inspired by low-temperature solution reactions down to −30 °C for metal chalcogenides such as Sb_2Te_3 and Bi_2Te_3 using alkylsilyl compounds $(R_3Si)_2M$ as precursors, where M denotes chalcogenes, and the symbol R designates an alkyl group [28]. Such an approach should result in the formation of stoichiometric compounds with minimal amounts of thermally activated defects, rather relying on the chemical reaction of the precursors. The global reaction for Bi_2Te_3 is as follows: $2BiCl_3(g) + 3Te(SiMe_3)_2(g) \rightarrow Bi_2Te_3(s) + 6Me_3SiCl(g)$.

As mentioned above, the structure of Bi_2Te_3 is highly anisotropic and defining the growth modes is expected to be difficult. Remarkably, we found that three different growth modes are possible by controlling the nucleation kinetics and/or employing the epitaxial substrates: (i) polycrystalline growth via dense, random nucleation and growth, (ii) van der Waals epitaxy on SiO_2/Si substrates by suppressed nucleation events, resulting in the CVD graphene-like texture, (iii) hetero-epitaxy on single crystalline Al_2O_3 and GaAs substrates. The detailed growth behaviors will be reported elsewhere. In this study, we focus on the results of the polycrystalline growth mode and on the implication of fine-tuned grain size and defect activation on thermopower engineering.

Top-view SEM micrographs in figures 1(*a*)–(*d*) show a clear evolution of the grain growth in the range of ∼50–∼200 nm in average diameter (D_{avg}) by increasing the growth temperature during ALD (T_{sub}, 100–160 °C in this study, including 220 °C results as a control). More interestingly, the grain growth in the resulting D_{avg} is apparent even with increasing 10 °C as proved by AFM (figures 1(*e*)–(*g*) and (*j*)). Although D_{avg} looks uniform when observed in a top view, its distribution became significant in the samples grown at over 140 °C (figure 1(*h*) and the inset of figure 1(*i*)), probably as a result of anisotropic grain growth. Indeed, the development of the *ab*-planes whose direction is perpendicular to the substrate is evident (figures 1(*d*) and (*i*)). Such an effect might be apparent in the growth rate as well (figure 1(*k*)). In general, the ideal ALD growth is believed to have a minimal temperature dependence because the thermal decomposition of precursors is avoided and it takes place in the self-limiting regime. As for the amorphous materials by nearly ideal ALD reactions, thus, this would be true in the whole ALD temperature window. However, it should deviate in crystalline materials with a high anisotropy such as metal chalcogenides when they randomly (or epitaxially) grow as shown in figure 1(*k*). Nonetheless, the possible contribution of thermal activations for surface diffusions could not be ruled out at the current stage.

The resulting structures were investigated by XRD and HR-TEM. Figure 2(*a*) shows the XRD results of ALD Bi_2Te_3 layers grown at different T_{sub}, showing mostly low-intensity peaks, i.e., (0,0,0,3n) according to the powder diffraction data (JCPDS no. 150863), and indicative of the anisotropic nature of Bi_2Te_3. The development of a high order peak (at around 57°) out of the 100% peak (015) implies the formation of a polycrystalline structure rather than a textured structure. This was testified in the morphologies as shown in figures 1(*d*) and (*i*). An HR-TEM image taken at a sample grown at $T_{sub} = 160$ °C exhibits the layered Bi_2Te_3 with grain boundaries (figure 2(*b*)). XPS results (data not shown here) showed the presence of surface oxides although HR-TEM testified no detectable impurity phases within the films ($T_{sub} =$ 100–160 °C). However, the XPS result is reliable due to the high sensitivity of Bi_2Te_3 toward surface oxidation reactions. Note that the energy-dispersive x-ray spectroscopic (EDX) elemental analysis is not applicable for such a material in that it is a line compound whose permeable dopants are much less than the detection errors (⩽5%) of EDX.

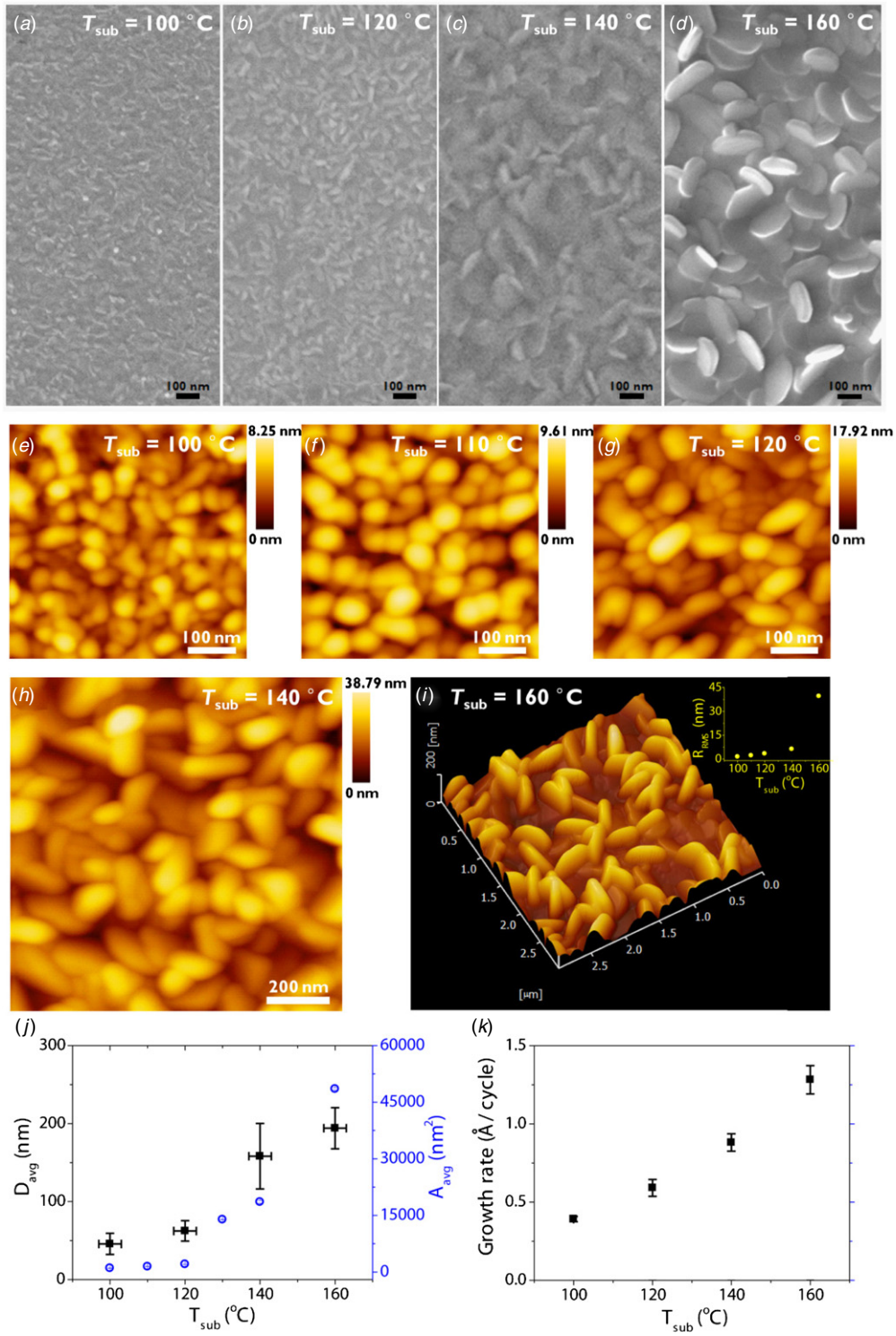

Figure 1. Surface analysis of Bi_2Te_3 layers grown at different T_{sub}. Top-view SEM micrographs at (*a*) T_{sub} = 100 °C, (*b*) 120 °C, (*c*) 140 °C, and (*d*) 160 °C. AFM height images at (*e*) T_{sub} = 100 °C, (f) 110 °C, (*g*) 120 °C, (*h*) 140 °C, and (*i*) 160 °C. The inset of panel (*i*) shows a plot of root mean square roughness (R_{RMS}) versus T_{sub}. (*j*) Plots of the average diameter (D_{avg})/the average grain area (A_{avg}) versus T_{sub} and (*k*) the growth rate versus T_{sub}.

The thermopower characterization began by patterning Hall bar structures in the resulting Bi_2Te_3 films, followed by metallization of Pt contacts. The device configuration essentially utilizes the Hall bar structure and the Pt resistance micro-heater located at the distal end of Bi_2Te_3 patterns. Then, the electrodes were connected to external circuits by aluminum bond-wires. The schematic depiction and the resulting device structures are shown in figure 3(*a*)–(*c*). The electrical transport properties could be understood by a combination of both the conductivity (figure 4(*a*)) and the Seebeck coefficient trends (figure 4(*b*)) from 50–400 K. All samples showed the metallic conduction (decrease of σ with temperature), except for the

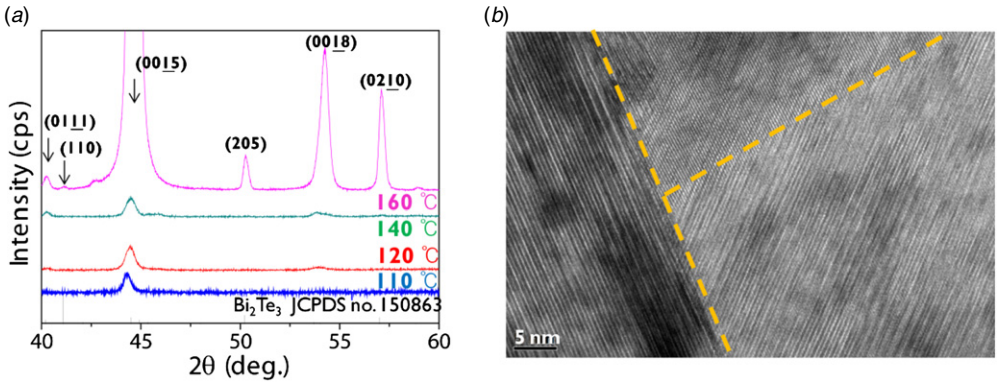

Figure 2. (*a*) XRD results of Bi_2Te_3 films grown at different T_{sub} and (*b*) TEM image of a sample at $T_{sub} = 120$ °C, showing the grain boundaries (dotted yellow line) and the layered structures of Bi_2Te_3, a quintuple ∼1 nm.

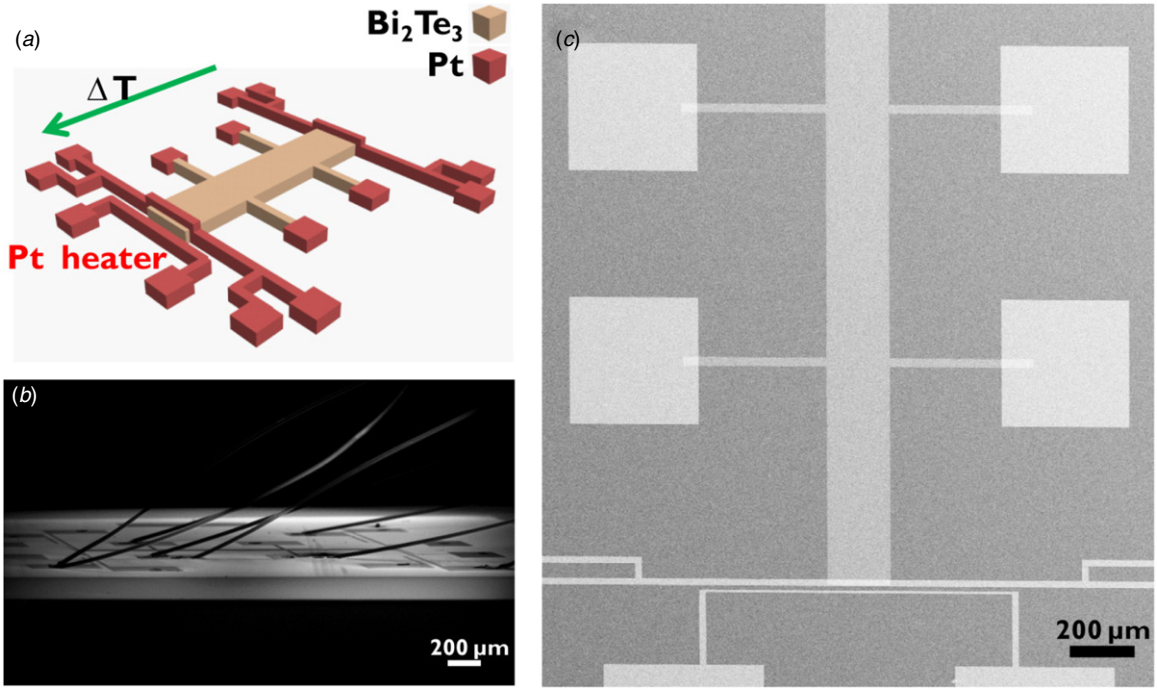

Figure 3. Device configuration used in this study. (*a*) Schematic illustration, (*b*) tilted-view and (*c*) top-view SEM of a representative device.

samples grown at $T_{sub} = 120$ °C (marked with open red circles in figure 4(*a*)). Figure 4(*b*) exhibits that the sample grown at ($T_{sub} = 100$ °C) has dominant *p*-type carriers by demonstrating the sign to be positive. The sign was calibrated by metallic Ni samples. This is reminiscent of the intrinsic *p*-type doping in the stoichiometric Bi_2Te_3 by Bi'_{Te} anti-site defects. We therefore conclude that the lowest $T_{sub} = 100$ °C produces the intrinsic *p*-type Bi_2Te_3 as was expected. In terms of the carrier concentration, the resulting samples were highly doped by observing the metallic conduction in the temperature ranges (exception at 120 °C, marked with red circles) (figure 4(*a*)). It is assumed that the amounts of carrier concentration are proportional to those of the thermally activated defects. The samples at $T_{sub} > 120$ °C exhibited a sudden conversion in their *S* values, indicative of dominating *n*-type doping in Bi_2Te_3 (figure 4(*b*)). This is explained by Te deficiency due to evaporation at higher temperatures. The degree of doping for these cases was also manifested as the magnitude of σ (almost one order for each) (see, yellow arrows in figure 4(*a*)). Indeed, the defect activations were systematically controlled from 120 through 140–160 °C while the grain sizes are kept at the nanoscale. The impurity levels within the band gap were estimated using an Arrhenius plot: $1/\sigma \sim e^{E_a/k_B T}$ where E_a is the activation energy and k_B is the Boltzmann constant. E_a of ∼35 meV was extracted out of the non-metallic sample ($T_{sub} =$ 120 °C), indicative of *n*-type shallow levels (figure 4(*d*)). Thus, such a type of impurity/defect levels is thought to be responsible for all of the *n*-type films. The maximum |S| for both signs were achieved in $T_{sub} = 100$ °C for *p*-type and 140 °C for *p*-type, respectively. Following such a trend, the highest power factor ($PF = S^2\sigma$) was found in the samples grown at $T_{sub} = 140$ °C (figure 4(*c*)). The observation is likely consistent with the fact that the moderate carrier doping leads to optimum thermoelectric performance [2].

More remarkably, our results highlight that the topological insulators with low carrier concentrations can be produced

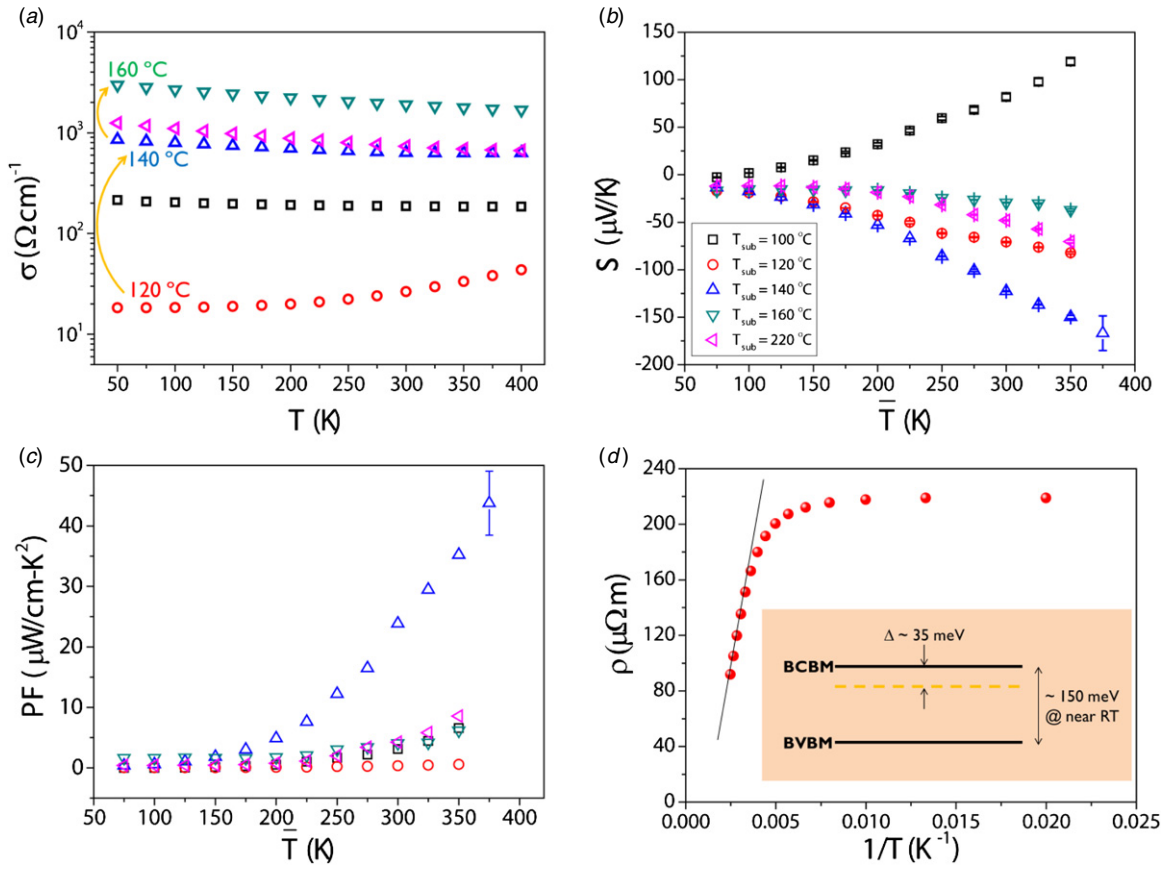

Figure 4. Electrical and thermoelectric characterization of our Bi_2Te_3 thin films grown at different T_{sub}. (*a*) The electrical conductivity σ, (*b*) the Seebeck coefficient S, (*c*) the power factor PF, and (*d*) an Arrhenius plot ($T_{sub} = 120$ °C), extracting a impurity level below the bulk conduction band minima (BCBM). All figures share with the symbols/colors as in the inset of panel (*b*).

alternatively to the classical alloying strategy. Indeed, the binary end compounds such as Bi_2Te_3 by high temperature processing should be inevitably degenerated as explained above. Otherwise, they have been produced with inhomogeneous doping/defects profiles. By this route, the large amounts of thermally activated defects are avoided in both of the applications, i.e., thermoelectric materials and topological insulators. To our knowledge, the present work is the first systematic study on the controlled defect activation in Bi_2Te_3 from low temperatures. The preparation at thermal equilibrium is also guaranteed due to the layer by layer and slow growth nature of ALD. From Fick's laws of diffusion ($L = (Dt)^{1/2}$), where D is the diffusion coefficient [$D^{Te} = 10^2$–10^4 exp(−1.7–2 eV kT^{-1}) cm$^2 \cdot$ s^{-1}] [19], we could estimate the diffusion time, t, to reach the equilibrium of the system. Combining the growth rate (figure 1(*k*)) with the results on n-type doping above 120 °C, furthermore, we were able to conclude that our Bi_2Te_3 was prepared at thermal equilibrium. Finally, we have shown that the resulting σ can systematically be tuned by several orders of magnitude, keeping the grain size within a very narrow D_{avg} (yellow arrows in figure 4(*a*)).

Control experiments at higher T_{sub} (>220 °C) revealed that the resulting Bi_2Te_3 layers were grown to be more textured even on SiO_2/Si substrates, i.e., c-plane mostly parallel to the substrate in-plane. The overall σ at $T_{sub} = 220$ °C was rather decreased when compared to that at $T_{sub} = 160$ °C (pink triangle, figure 4(*a*)) although enhanced σ is expected. XRD results (not shown here) indicated possible phase segregation at grain boundaries by detecting metallic bismuth. This explains the reduced σ originating many phase boundaries. Defect structures associated with grain/phase boundaries have not been considered here as well. Therefore, further study is needed in order to elucidate/correlate the structural details to thermoelectric properties.

4. Conclusion

In summary, we have successfully prepared polycrystalline, dense Bi_2Te_3 thin films by ALD at relatively low T_{sub}, and the grain sizes were finely tuned. We also measured the conductivity, Seebeck coefficient, and power factor of the films at a temperature range of 50–400 K. The interplay between nanostructuring and defect activation was elucidated in terms of the thermopower engineering. Remarkably, we observed the gradual defect activation with increasing T_{sub} from the nominal p-type to n-type in our Bi_2Te_3 without alloying. The present results demonstrate for the first time the possibility for thermopower engineering of Bi_2Te_3 without alloying, keeping the grain small and tuning the conductivity wide. They also revisit the optimization of thermoelectric materials not only by nanostructuring (i.e., phonon engineering) but also by controlled defect activation (i.e., electron engineering).

Acknowledgment

StS and KN gratefully acknowledge financial support by the DFG priority program 1666 'Topological Isolators'. StS would also like to thank the University of Dusiburg-Essen for funding. The study at Sungkyunkwan University was supported by the Human Resources Development program (no. 20124010203270) of KETEP grant funded by the Korean Government Ministry of Knowledge Economy, and by the Engineering Research Center program (CMPS: 2005-0049407).

References

[1] Heremans J P, Dresselhaus M S, Bell L E and Morelli D T 2013 *Nature Nanotechnol.* **8** 471
[2] Snyder G J and Toberer E S 2008 *Nature Mater.* **7** 105
[3] Hicks L D and Dresselhaus M S 1993 *Phys. Rev.* B **47** 16631
[4] Minnich A J, Dresselhaus M S, Ren Z F and Chen G 2009 *Energy Environ. Sci.* **2** 466
[5] Zebarjadi M, Esfarjani K, Dresselhaus M S, Ren Z F and Chen G 2012 *Energy Environ. Sci.* **5** 5147
[6] Shi L 2012 *Nanoscale Microscale Thermophys. Eng.* **16** 79
[7] Hsu K F, Loo S, Guo F, Chen W, Dyck J S, Uher C, Hogan T, Polychroniadis E K and Kanatzidis M G 2004 *Science* **303** 818
[8] Poudel B *et al* 2008 *Science* **320** 634
[9] Joshi G *et al* 2008 *Nano Lett.* **8** 4670
[10] Biswas K, He J, Blum I D, Wu C-I, Hogan T P, Seidman D N, Dravid V P and Kanatzidis M G 2012 *Nature* **489** 414
[11] Koumoto K, Wang Y, Zhang R, Kosuga A and Funahashi R 2010 *Annu. Rev. Mater. Res.* **40** 363
[12] Feser J P, Chan E M, Majumdar A, Segalman R A and Urban J J 2013 *Nano Lett.* **13** 2122
[13] Sootsman J R, Chung D Y and Kanatzidis M G 2009 *Angew. Chem. Int. Edn* **48** 8616
[14] Nielsch K, Bachmann J, Kimling J and Böttner H 2011 *Adv. Energy Mater.* **1** 713
[15] Hasan M Z and Kane C L 2010 *Rev. Mod. Phys.* **82** 3045
[16] Takahashi R and Murakami S 2012 *Semicond. Sci. Technol.* **27** 124005
[17] Austin I G and Sheard A 1956 *J. Electron. Control* **3** 236
[18] Fuschillo N, Bierly N J and Donahoe F J 1959 *J. Phys. Chem. Solids* **8** 430
[19] Miller G R and Li C-Y 1965 *J. Phys. Chem. Solids* **26** 173
[20] Ghoshtagqre R N 1967 *Phys. Rev.* **155** 598
[21] Jia S, Ji H, Climent-Pascual E, Fuccillo M K, Charles M E, Xiong J, Ong N P and Cava R J 2011 *Phys. Rev.* B **84** 235206
[22] Hong S S, Cha J J, Kong D and Cui Y 2012 *Nature Commun.* **3** 757
[23] George S M 2010 *Chem. Rev.* **110** 111
[24] Detty M R and Seider M D 1982 *J. Org. Chem.* **47** 1354
[25] Zastrow S, Gooth J, Böhnert T, Heiderich S, Toellner W, Heimann S, Schulz S and Nielsch K 2013 *Semicond. Sci. Technol.* **28** 035010
[26] Böhnert T, Vega V, Michel A-K, Prida V M and Nielsch K 2013 *Appl. Phys. Lett.* **103** 092407
[27] Pore V, Hatanpaa T, Ritala M and Leskela M 2009 *J. Am. Chem. Soc.* **131** 3478
[28] Groshens T J, Gedridge R W Jr and Lowe-Ma C K 1994 *Chem. Mater.* **6** 727

DOI: 10.1088/0268-1242/29/6/064003
URN: urn:nbn:de:hbz:464-20201117-103259-8